

Article

Concept and Design of a Velocity Compounded Radial Four-Fold Re-Entry Turbine for Organic Rankine Cycle (ORC) Applications

Philipp Streit ^{1,2,*}, Andreas P. Weiß ^{1,2}, Dominik Stümpfl ¹, Jan Špale ^{2,3,4} , Lasse B. Anderson ⁵,
Václav Novotný ^{2,3}  and Michal Kolovratník ²

¹ Centre of Excellence for Cogeneration Technologies, East-Bavarian Technical University of Applied Sciences Amberg-Weiden, Kaiser-Wilhelm-Ring 23, 92224 Amberg, Germany

² Czech Technical University in Prague, Faculty of Mechanical Engineering, Technická 4, Praha 6, 16607 Prague, Czech Republic

³ Czech Technical University in Prague, University Centre for Energy Efficient Buildings, Trinecka 1024, 27343 Bustehrad, Czech Republic

⁴ Ray W. Herrick Laboratories, School of Mechanical Engineering, Purdue University, 177 S Russel St., West Lafayette, IN 47907, USA

⁵ Department of Energy and Process Engineering, NTNU—Norwegian University of Science and Technology, NO-7491 Trondheim, Norway

* Correspondence: ph.streit@oth-aw.de

Abstract: The energy sector faces a pressing need for significant transformation to curb CO₂ emissions. For instance, Czechia and Germany have taken steps to phase out fossil thermal power plants by 2038, opting instead for a greater reliance on variable renewable energy sources like wind and solar power. Nonetheless, thermal power plants will still have roles, too. While the conventional multistage axial turbine design has been predominant in large-scale power plants for the past century, it is unsuitable for small-scale decentralized projects due to complexity and cost. To address this, the study investigates less common turbine types, which were discarded as they demonstrated lower efficiency. One design is the Elektra turbine, characterized by its velocity compounded radial re-entry configuration. The Elektra turbine combines the advantages of volumetric expanders (the low rotational speed requirement) with the advantages of a turbine (no rubbing seals, no lubrication in the working fluid, wear is almost completely avoided). Thus, the research goal of the authors is the implementation of a 10 kW-class ORC turbine driving a cost-effective off-the-shelf 3000 rpm generator. The paper introduces the concept of the Elektra turbine in comparison to other turbines and proposes this approach for an ORC working fluid. In the second part, the 1D design and 3D-CFD optimization of the 7 kW Elektra turbine working with Hexamethyldisiloxane (MM) is performed. Finally, CFD efficiency characteristics of various versions of the Elektra are presented and critically discussed regarding the originally defined design approach. The unsteady CFD calculation of the final Elektra version showed 46% total-to-static isentropic efficiency.

Keywords: turbine; radial; velocity compounded; re-entry; Elektra; ORC



Citation: Streit, P.; Weiß, A.P.; Stümpfl, D.; Špale, J.; Anderson, L.B.; Novotný, V.; Kolovratník, M. Concept and Design of a Velocity Compounded Radial Four-Fold Re-Entry Turbine for Organic Rankine Cycle (ORC) Applications. *Energies* **2024**, *17*, 1185. <https://doi.org/10.3390/en17051185>

Academic Editor: George Kosmadakis

Received: 24 January 2024

Revised: 23 February 2024

Accepted: 28 February 2024

Published: 1 March 2024



Copyright: © 2024 by the authors. Licensee MDPI, Basel, Switzerland. This article is an open access article distributed under the terms and conditions of the Creative Commons Attribution (CC BY) license (<https://creativecommons.org/licenses/by/4.0/>).

1. Introduction

The Rankine Cycle, employing steam, has served as a foundation for electricity generation for over a century and a half. In their initial stages, reciprocating steam engines drove generators, but they soon made way for more efficient steam turbines, enabling significantly higher power output per unit. By the late 20th century, the standard size for coal-fired or nuclear steam power plants reached approximately one gigawatt, utilizing multistage axial turbines as highly efficient expanders [1]. However, the modern era has seen shifts in energy production as some countries, e.g., Czechia and Germany, have chosen to abandon coal-based electricity generation in efforts to mitigate environmental pollution and combat climate change. Instead, alternative heat sources such as geothermal energy,

solar radiation, and industrial waste heat are being harnessed for electricity production, often in much smaller, decentralized units closer to consumers. This has led to the consideration of small Rankine power stations working with organic vapours (ORC), some even significantly below the one-megawatt range [2,3], especially in small industries or even residential micro-cogeneration.

Yet scaling down the multistage axial turbine concept to produce just one megawatt or even hundreds or dozens of kW is not reasonable, considering efficiency and specific costs. Thus, research and development of ORC small-scale turboexpanders has occurred in several institutes in the world (see Table 1). This is remarkable because many authors claim that volumetric expanders are best for those small power ratings; e.g., [4,5]. However, in contrast to turbines, volumetric expanders suffer from wear and tear due to the necessary rubbing contact surfaces. To mitigate this, a lubricant is necessary that spoils the organic working fluid. There are no rubbing contact surfaces in turbines, so no lubricant is needed. Due to the small built-in volume ratio ($VRAT \leq 10$), volumetric expanders are limited to rather small temperature differences between the heat source and heat sink. Turbines can be easily adjusted to almost any temperature or pressure ratio, respectively. For more details concerning the pro and cons of turbines, the reader is referred to [6].

Table 1 provides an exclusive summary of experimental research in ORC turboexpanders of a small scale (of under 50 kW_{el} power output) in the available literature. Please note that in some publications, the reported efficiency is not evaluated from measured power output, but only from measured inlet and outlet enthalpy, which is known to overestimate the real value for small-scale systems, so these numbers are indicative rather than conclusive. These values are marked by an asterisk. Refer to the reference for the detailed list of boundary conditions of the experiment.

Almost half of the investigations apply axial impulse turbines, while the other half of the investigations apply radial inflow turbines with rather modest pressure ratios ($PR < 10$)—exception [7,8]. Most studies, therefore, use classic single-stage turbine architectures (axial and radial-inflow-axial-outflow turbines). Here, the exceptions are [9] with a four-stage arrangement and [7,10] with radial inflow-radial-outflow cantilever turbines. In order to reduce the typically high rotational speed demand of small turbines, Sun et al. [11] followed the approach of extreme partial admissions ($\varepsilon = 3.3\%$). A partial admission means that only a portion of the wheel's arc is submitted to the flow. This allows for bigger wheel diameters and, therefore, lower rotational speeds [6]. The newest turbine architecture is the so-called ROT radial outflow turbine [12,13], which can cope with a high pressure ratio thanks to a radial multistage arrangement.

Table 1. Summary of the experimental investigations of ORC turboexpanders of micro-scale power output (<50 kW_{el}). An Asterix (*) indicates that the power is calculated from measured inlet and outlet enthalpy rather than directly measured.

Reference	Working Fluid	Turbine Type	PR	P _{el} [kW]	η_{is} [%]
Kaczmarczyk et al. [9]	HFE7100	4-stage radial axial	7	2	70
Zywica et al. [14,15]	HFE7100		3.1	1	73
Riffat & Zhao [16]	n-pentane	Axial	5	3.7	n.a.
Hernandez-Carillo [17]	R245fa	Radial inflow	n.a.	1.2	66
Pu et al. [18]	R245fa; HFE7100	Axial	3.5	2	60
Li et al. [19]	R123	Axial	6.3	6.1	58.5
Pei et al. [20]	R123	Radial inflow	7.5	3.3	66
Nguyen et al. [21]	n-pentane	Radial inflow	4.1	1.5	50
Yagoub et al. [22]	HFE-301	Radial inflow	n.a.	1.5	85 *
Yagoub et al. [22]	n-pentane	Radial inflow	n.a.	1.5	40
Klonowicz et al. [23]	R227ea	Axial impulse	2.9	10.1	59
Shao et al. [24]	R123	Radial inflow	3	3.4	83.6 *
Seume et al. [25]	Ethanol	Axial impulse	50	8	58
Kosowski et al. [26]	Ethanol	Axial impulse	17.3	2	n.a.

Table 1. Cont.

Reference	Working Fluid	Turbine Type	PR	P _{el} [kW]	η_{is} [%]
Weiß et al. [7]	MM	Axial impulse; radial cantilever	18.8	14.1 16	73.4; 76.8
Rosset et al. [27]	R245fa	Radial inflow	3–4.5	2.3	77
Popp et al. [10]	MM	Radial cantilever	14	12	64
Uusitalo et al. [8]	MDM	Radial inflow	60–80	10	70
Gazet et al. [28]	HFE	Axial impulse	3	10	70
Yue et al. [29]	R245fa	Axial	n.a.	5	56.4
Guillaume et al. [30]	R1233zd	Radial inflow	4	3.5	75
Demierre et al. [31]	R134a	Radial inflow	4.3	2.4	67
Cho et al. [32]	R245fa	Axial	4.8	2.2	n.a.
Al Jubori et al. [33]	various	Radial inflow	1.2–2.2	4.8	78.3
Bahamonde et al. [12]	MM	Radial outflow	35.2	10	68.7
Casati et al. [13]	D4	Radial outflow	45	10.3	77
Sun et al. [11]	R1233zde	Axial impulse Partially admitted	3.5	0.6	35.8

The authors of this paper have developed a micro-turbine construction kit (MTG-c-kit) [34] based on a straightforward partially admitted impulse turbine design. In an impulse turbine, the entire stage enthalpy drop is converted into kinetic energy already in the nozzles or stationary vanes, respectively. The single-turbine wheel is directly integrated with the generator shaft, creating a hermetically sealed turbo-generator unit. Thus, no additional bearings and no coupling is required. The basic architecture can be easily adjusted to different working fluids and pressure (i.e., temperature) ratios. The achieved total-to-static isentropic efficiencies in small test turbines (ranging from 5 kW to 15 kW, with $60\% < \eta_{is,ts} < 75\%$) have proven to be satisfactory [34]. However, these turbines demand high rotational speeds (ranging from 20,000 rpm to 50,000 rpm) and, thus, necessitate high-speed generators (highly exceeding standard 3000 rpm) [3], which contribute significantly to the specific cost of the entire turbo generator (ranging from 1000 €/kW_{el} to 1500 €/kW_{el}). To mitigate this cost challenge, the authors are exploring the potential of velocity compounding. Velocity compounding, a concept previously used in Curtis turbines [35] during the early days of electrification in the 20th century, offers a way to decrease the necessary circumferential velocity u for a particular stage enthalpy drop Δh and consequently reduces the rotational speed n . Just as in the impulse stage, the total stage enthalpy drop is converted to kinetic energy in the nozzles. But a Curtis turbine with two velocity stages reduces the speed requirement to 50% (see Table 2), and a turbine with four velocity stages reduces it to 25% of a single impulse stage. In an axial Curtis turbine arrangement, this means one additional or three additional bucket wheels. Although velocity compounding provides less efficiency potential compared to pressure compounding, it holds promise in the context of small, decentralized power generation. In this approach, the possibility to use an off-the-shelf (i.e., standard) generator (1500–3000 rpm), with its cost advantage, may offset any efficiency disadvantages when comparing the overall long-term performance of the unit. Furthermore, a lower efficiency might not be crucial because the dumped heat can be used for following heating or cooling purposes in a cogeneration regime [36–39].

Table 2. Comparison of required optimal circumferential speed u_{opt} as a function of the number of velocity stages.

	Impulse Turbine	Curtis, Two Velocity Stages	Curtis, Four Velocity Stages
u_{opt}	$\left(\frac{\Delta h_{is}}{2}\right)^{0.5}$ 100%	$\frac{1}{2} \left(\frac{\Delta h_{is}}{2}\right)^{0.5}$ 50%	$\frac{1}{4} \left(\frac{\Delta h_{is}}{2}\right)^{0.5}$ 25%

To maintain the advantages of a single turbine wheel directly mounted on the generator shaft (MTG-c-kit), the velocity compounding must be implemented in radial i.e., centripetal flow direction. For instance, Klonowicz et al. [40] discuss a radial Curtis turbine with two velocity stages. However, for achieving 3000 rpm in a 10 kW_{el} rating range for testing, four velocity stages are necessary. This can be accomplished by combining velocity compounding with the re-entry (RE) concept. Figure 1 illustrates the geometry of the radial four-fold re-entry turbine (RFFRE-T) developed and investigated in the current research project. The working fluid enters the turbine radially (Turbine inlet) and is accelerated in the convergent-divergent (CD) nozzle. The first pass of the buckets (first WP, Figure 1) occurs centripetally in the transonic flow regime. Downstream, the flow is redirected by the first deflection channel (white arrows). It enters the buckets a second time centrifugally (second WP) and is redirected again. This is repeated for a third and a fourth wheel pass (third and fourth WPs). The total-stage enthalpy drop is converted to approximately 45% in the first wheel pass, 30% in the second, 19% in the third, and, finally, 6% in the fourth pass according to our 1D design calculations discussed below. The total mass flow rate is distributed on two parallel-working flow paths (Figure 1).

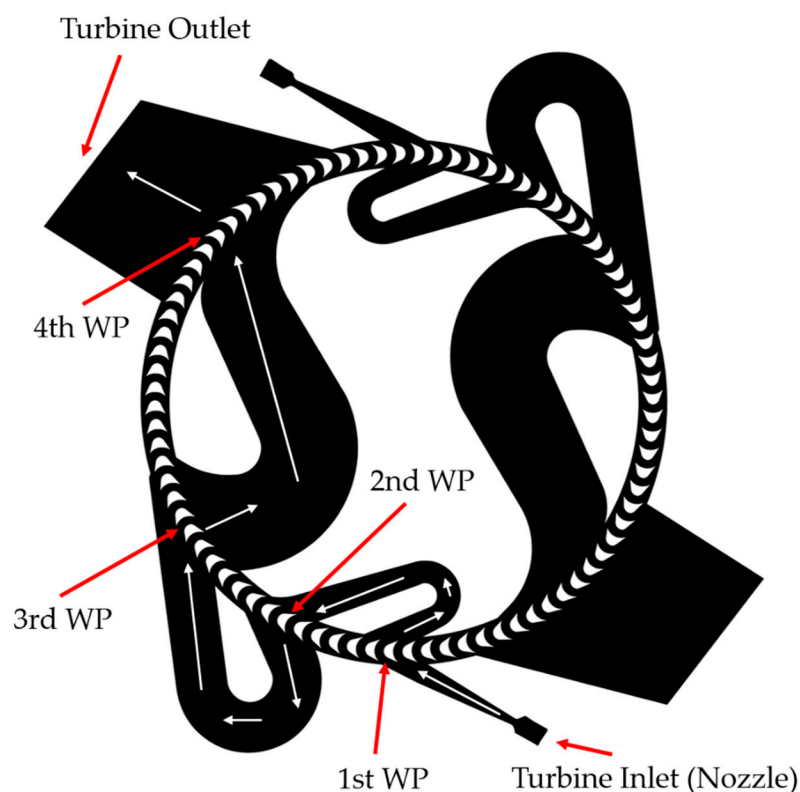


Figure 1. Turbine with the flow direction shown with white arrows and wheel passes (WP) with red arrows.

In the first decades of the 20th century, radial RE turbines, referred to as “Elektra Turbines”, were relatively common [41–43]. These turbines were utilized in various applications, such as on ships, where they operated pumps and fans at speeds ranging from 1000 to 3000 rpm. Despite their efficiency being relatively modest at around 30% [44], it was acceptable since the exhaust steam (or heat) released could be directly utilized e.g., for purposes like pre-heating within the ship’s steam systems.

In the opinion of the authors, the velocity compounded radial RE-turbine architectures, which might allow for the implementation of an easily adjustable and cost-effective 3000 rpm turbo generator for small-scale distributed power generation using Organic Rankine Cycle units. Consequently, the primary objectives of the current research project, based on the existing knowledge, can be summarized in three main questions:

1. Is it feasible to develop an ORC-Elektra turbine that drives an off-the-shelf (i.e., standard) generator operating within the range of 1500–3000 rpm and delivers an isentropic expansion efficiency of at least 50%? The initial Elektra designs from the early 20th century that operated with steam, as documented [43,44], achieved efficiencies significantly below 50% for power ratings exceeding 30 kW. Nevertheless, the researchers of that era did not have access to today's computational fluid dynamic (CFD) tools, which are expected to offer significant room for improvements, especially in the design of deflection channels.
2. Is it possible to significantly reduce the manufacturing and operational costs of a small-scale ORC expanders thanks to the velocity-compounding RFFRE-T (i.e., Elektra) concept? The Elektra turbine combines the advantages of volumetric expanders (the low rotational speed requirement) with the advantages of a turbine (no rubbing seals, no lubrication in the working fluid, wear is almost completely avoided, etc. [6]).
3. What is the lowest power rating at which the above-mentioned objectives can be met effectively?

Despite the overall potential of velocity-compounded turbines, especially the RE concept, for cost-effective small-scale turbo generators, this concept has remained largely unexplored since the 1960s [45–47]. To the best of the authors' knowledge, there is only one recent publication [48]. However, the landscape of power systems has transformed dramatically since the middle of the last century, necessitating fresh or even disruptive approaches. Additionally, the availability of new design and manufacturing techniques like 3D flow simulations and 3D printing present an opportunity to re-examine the velocity-compounded radial RE-turbine concept. The present study represents a rare application of these modern methods to the development of such an Elektra turbine, with the aim of addressing the open question of whether, with these advanced tools, it is currently viable to create an ORC turbo generator that is both competitive in terms of efficiency and superior in terms of specific costs.

Due to the potential of this concept, the authors first designed and investigated several compressed air Elektra demonstrators [49], equipped with two velocity stages. Based on the gained experience, the authors have currently developed a 7 kW_{el} velocity-compounded radial four-fold RE turbine for application in an existing small CHP–ORC plant working with Hexamethyldisiloxane (MM). The plant is providing heat and power for the University Centre of Energy Efficient Building (UCEEB) at the Czech Technical University in Prague (CTU). Currently, a rotary vane expander is driving the generator. In the following, the Elektra design considerations, the design approach, and the optimization by computational fluid dynamics (CFD) are presented and discussed.

2. Methodology

The examination of the Elektra turbine, as detailed in this article, adhered to design procedures (Figure 2) proven in the development of other turbomachines [7,49,50]. Commencing with the provided input data and boundary conditions (which will be described subsequently), we initially determined the preliminary flow path geometry of the turbine using our in-house 1D Turbine Design Tool (1DTDT). Subsequently, we translated the geometry parameters into a computer-aided design (CAD) model.

Building on this CAD model, we conducted numerical investigations through 3D computational fluid dynamic (CFD) simulations. These simulations played a pivotal role in fine-tuning the geometry, and this was achieved through an iterative process. Depending on the complexity of the changes required in the geometry, adjustments were either directly implemented within the CFD environment or were first modified in the CAD software PTC Creo 7.0. The specific steps of this design and optimization process are elucidated in greater detail below.

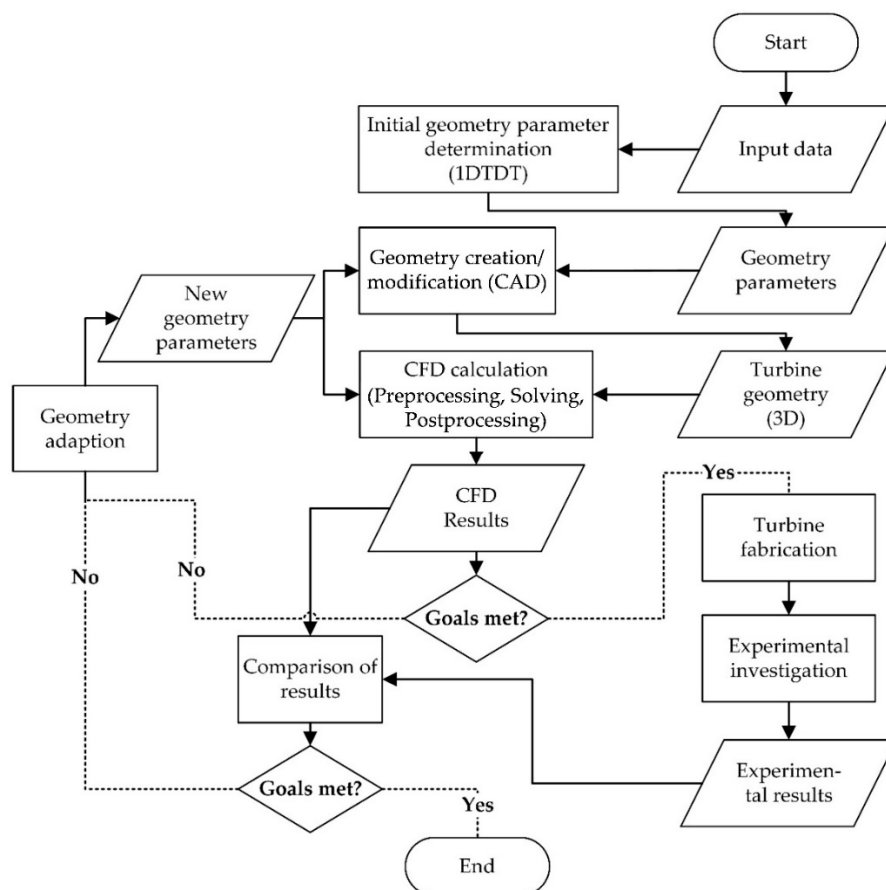


Figure 2. Workflow of the Elektra-turbine investigation [49].

The lower right-hand branch of Figure 2, the fabrication and experimental investigation, is an integral part of our design loop. However, it will not be discussed in this paper, but it will be presented and discussed in a future publication after its implementation.

2.1. 1D Turbine Design

The 1D Turbine Design Tool (1D TDT) offers a rapid means of calculating geometry data, power output, and turbine efficiency for various turbine types, including axial impulse, two-wheel velocity-compounded Curtis turbines, and radial cantilever quasi-impulse turbines. This MS Excel-based software (Version 1808) utilizes a 1D mean line model and a proprietary loss model [50] to perform these calculations. Additionally, it allows for the evaluation of radial-inflow-axial-outflow reaction turbines, employing an open-access loss model introduced in [51]. For further details about the loss models applied, readers can refer to [50].

The tool relies on REFPROP fluid properties [52] to determine the thermodynamic properties of the chosen working fluid. Building upon the existing 1D Turbine Design Tool (1D TDT), recent developments have expanded its capabilities to include the design of velocity-compounded RFFRE-T in a one-dimensional framework. Although the procedure has been previously outlined in [49], it is reiterated here for comprehensive understanding.

To commence the iterative design process (as detailed in Figure 2), specific parameters must be defined, including the working fluid, inlet total conditions, required mass flow rate, and static exit pressure. Additionally, an evaluation of the total-to-static isentropic expansion efficiency is essential for establishing the static outlet conditions of the final wheel pass (refer to Table 3). In two former research projects, the authors already designed and tested small MM-ORC turbines for quite similar boundary conditions [7,34]. The tested turbines were all impulse types with one wheel pass. They were equipped with 120 mm bucket wheels and required a rotational speed of about 25,000 rpm. By applying a four-fold

velocity-compounded RE turbine for four-wheel passes, the necessary rotational speed can be reduced to approximately 25%, i.e., 6000 rpm (see Table 2). To achieve 3000 rpm, the wheel diameter must be at least doubled (a 255 mm diameter was selected for this case) (Table 3).

Table 3. Input data for the 1DTDT with corresponding values for the Elektra turbine.

Input Data	Unit	Elektra Turbine
Working fluid	-	MM
Total inlet pressure	kPa	650
Total inlet temperature	K	463
Required mass flow rate	kg/s	0.303
Static exit pressure	kPa	55
Wheel diameter, D_{out}	m	0.255
Wheel diameter ratio, D_{in}/D_{out}	-	0.90
Final wheel pass degree of admission	%	50
Rotational speed, n	rpm	3000
Estimated expansion efficiency	%	40.0

The specified thermodynamic parameters (Table 3) correspond to the operational data of the woodchip-fired CHP plant at the University Centre for Energy Efficient Buildings (UCEEB), Czech Technical University in Prague (CTU) [53,54], in which the Elektra technology demonstrator is to be tested after the mechanical design is finished and the system is manufactured.

The design and optimization of the wheel or turbine buckets are restricted to a single flow pass, meaning that factors like diameter, diameter ratio, blade angles, blade height, and the number of blades can only be configured for one specific flow pass. Since the first wheel pass converts the highest enthalpy drop, the configuration is done for the first pass. Similarly, the circumferential speed (denoted as “ u ”) is consistent for all the passes. For subsequent passes, “design” becomes more of an analysis rather than a traditional design calculation.

In this context, the approach is to initiate the calculations from the exit pressure of the last wheel pass and then work in a reverse manner. This involves determining the flow velocity, velocity triangle, and total and total relative thermodynamic conditions at the wheel exit. Then, based on available loss models [50], enthalpy losses are assessed to compute the flow velocity, velocity triangle, and total and total relative thermodynamic conditions at the wheel’s inlet. If there is a nozzle upstream of the wheel pass, such as a supersonic CD nozzle, it can be calculated, considering parameters like flow area and length using a simple loss correlation [50]. The CD nozzles have a rectangular cross-sectional area, with the divergent section featuring straight walls, making them easy to manufacture and reliable [7].

When a deflection channel is present upstream of the wheel pass, the channel’s design involves calculating flow areas to maintain constant pressure. This calculation considers enthalpy dissipation, which varies with the Mach number and deflection angle, such as a blade row. Since the deflection angle depends on the absolute inlet angle at the specific wheel pass and the absolute exit angle of the wheel pass immediately upstream, this task cannot be resolved purely analytically and necessitates an iterative approach.

The design of the turbine blade wheel is a combination of experience-based decisions and design considerations. The outer diameter D_{out} is determined with consideration for the desired or feasible maximum rotational speed. The diameter ratio D_{in}/D_{out} should be close to unity (approximately 0.90) to minimize the unnecessary addition and extraction of pumping work by the centrifugal pressure field for each wheel pass. The blade angles of the impulse buckets ($\beta_{out} = 180^\circ - \beta_{in}$) typically fall in the range of approximately 30° (see Figure 3). With the known mass flow rate and the known thermodynamic outlet conditions, the unknown blade height can be determined considering the outlet diameter of the final wheel pass and the blade angle.

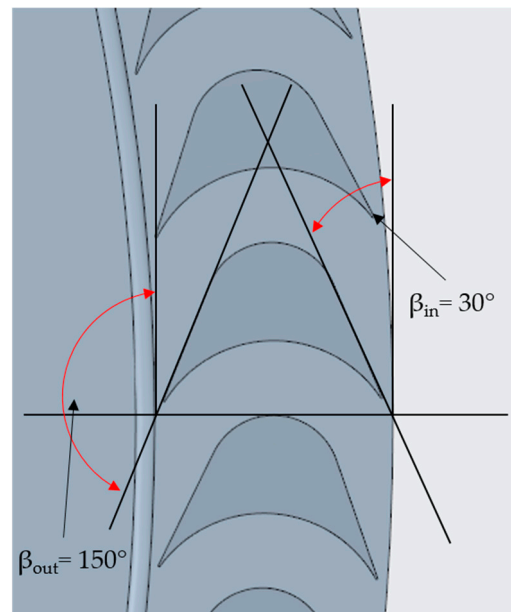


Figure 3. Bucket inlet and outlet blade angles (red arrows).

Since the flow passes the wheel via the outer and the inner diameter, the inner and outer circumferential surface should be equal to what results in the requirement for the blade heights: $h_{out}/h_{in} = D_{in}/D_{out}$.

As a result of velocity compounding, both absolute velocity and its radial component decrease from one wheel pass to the next (see Figure 4). This necessitates an increase in the degree of admission ε (see Figure 1, portion of the arc which is submitted to flow), or the flow area of the deflection channels as one progresses from pass to pass. Moreover, with the diminishing radial velocity component, the angle α between the absolute velocity c and the circumferential velocity u becomes smaller, as the relative flow angle β (\approx metal blade angle, Figure 3) and the circumferential velocity u remain constant (Figure 4). Therefore, the final nozzle's inclination to the circumferential direction u will be higher ($\approx 25^\circ$) than the usual $12\text{--}15^\circ$ observed in classical impulse or axial Curtis turbine stages.

While the designed wheel maintains a constant area $A_{in} = A_{out}$ ($\pi D_{in} h_{in} = \pi D_{out} h_{out}$), friction and boundary layers impact the process, resulting in profile and secondary losses. When dealing with relative flow Mach numbers below unity, the flow accelerates, leading to a pressure drop. Conversely, for relative Mach numbers exceeding unity, the flow decelerates, resulting in a pressure increase. Consequently, despite the design principles of an impulse wheel ($\beta_{out} = 180^\circ - \beta_{in}$, $A_{in} = A_{out}$), a pressure change occurs for each wheel pass. Multiple internal and external iterations are required to achieve the specified total inlet pressure for the particular mass flow rate and to align the calculated expansion efficiency with the initially assessed value.

Based on these considerations and assumptions, the authors have designed and tested their first Elektra turbine demonstrators with pressurized air [49]. The experimental results have been fed back into the design procedure (Figure 2). As a consequential step, the authors have started the development of a 3000 rpm MM-Elektra turbine for ORC-WHR applications.

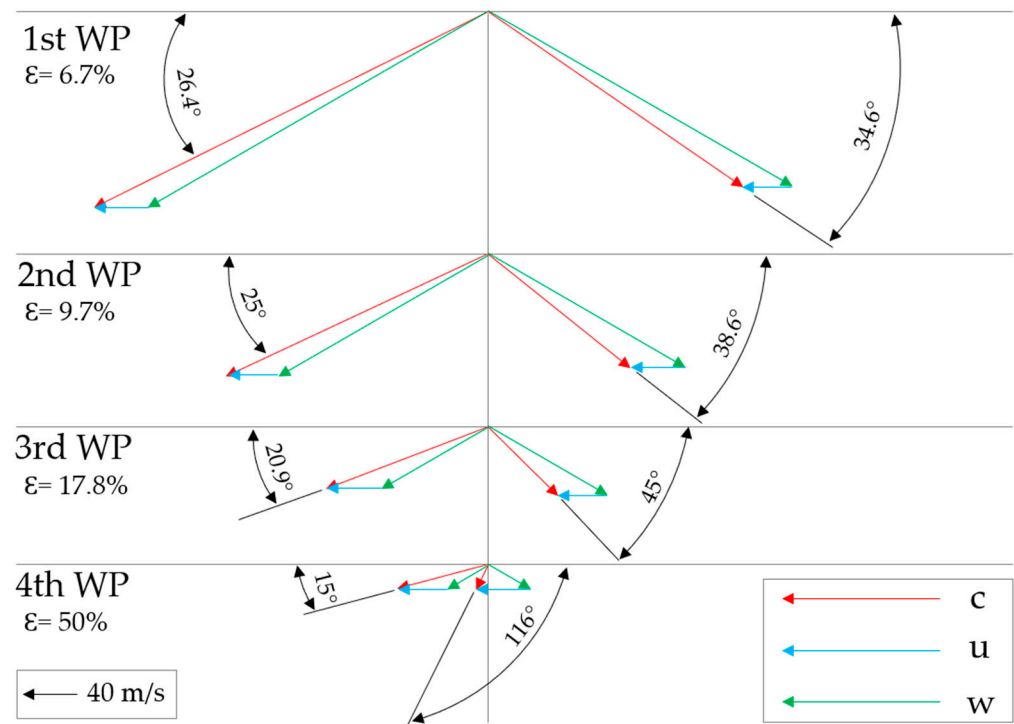


Figure 4. Velocity triangles of the velocity compounded RFFRE-T for MM (absolute velocity c , relative velocity w , circumferential velocity u).

2.2. CFD Settings

For the CFD Simulations, the FineTM/Turbo package from Cadence, San Jose, CA, USA [55], specifically the EURANUS flow solver, which operates on Reynolds-averaged Navier–Stokes (RANS) equations and utilizes multiblock-structured grids, was employed. More details regarding the flow solver can be found in Hirsch et al. [56] and Jameson et al. [57].

The essential input data for the FineTM/Turbo simulations, including the models and boundary conditions, are detailed in Table 4. The primary objective was to attain reliable numerical results within an appropriate computational timeframe. This was achieved by solving the RANS equations, in combination with the Spalart–Allmaras turbulence model. The MM fluid data were calculated by REFPROP and stored in a look-up table.

Table 4. Physical models and boundary conditions of the CFD simulations.

Model or Condition	Parameter
Mathematical model	RANS
Turbulence model	SA with EWF
Rotor–stator interface	Full non-matching frozen rotor
Walls definition	Solid, adiabatic
Efficiency definition	Total-to-static isentropic
Fluid model	MM (REFPROP Fluid Database)
Inlet boundary conditions	Absolute total pressure $p_0 = 650$ kPa Total temperature $T_0 = 463$ K
Outlet boundary condition	Averaged static pressure $\bar{p}_{out} = 55$ kPa
Rotational speed (Constant)	3000 rpm

Figure 5 depicts the simulation model outcome for the Elektra turbine. The block structure of the inlet and the CD nozzle is shown in yellow, the rotor wheel is shown in green, the deflection channels are shown in red, and the outlet is shown in light blue. Between the stator parts and the rotor, the rotor–stator–interface in dark blue can

be seen. Utilizing its rotational symmetry, it was possible to reduce the simulation model on a 180° section of the turbine, a measure taken to optimize the computational efficiency. The radial gaps between the rotor and stator components were represented in the model, but to simplify the 3D Computational Fluid Dynamic (CFD) simulation, which was used to achieve the design calculations' turn-around time of 1 day, the gaps at both the hub and shroud were not modeled. Consequently, any losses stemming from fluid circulation and flows along the outer regions of the wheel's hub and shroud were not included in the analysis. Additionally, discontinuities in channel height between the rotor and stator, stemming from manufacturing tolerances, were also not considered. These simplifications have already been implemented for the simulations of the compressed air turbines and turned out to be very efficient for the design optimization loops, which is why a simplified mesh is also used in this work.

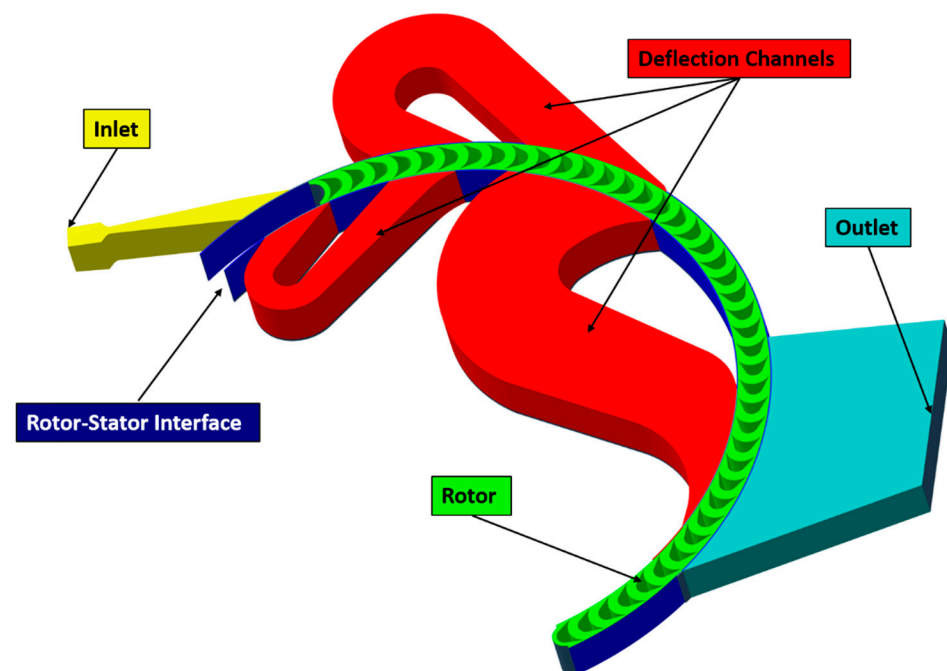


Figure 5. Simulation model of the Elektra turbine (half mesh due to symmetry plane).

In order to assess the mesh's quality, a mesh study was conducted. Figure 6 illustrates the deviation of the inlet and outlet mass flow rates, as well as the total-to-static isentropic efficiency based on the number of grid points in millions. The mass flow rate through the turbine consistently remained in the range of approximately 300 g/s to 302 g/s. The coarsest mesh, at around 2.5-million grid points, had the highest deviation of 1.8%, with 300.54 g/s at the inlet to 294.99 g/s at the outlet. The deviations in the mass flow rate decreased as the mesh became finer. At around 20-million to over 30-million grid points, the deviation remained at a very low level of 0.1%. The efficiency was at around 46.5% for the coarsest grid and at around 48% for the finest grid. After 20.63-million grid points, the efficiency seemed to converge at an efficiency of around 47.7%. Through this evaluation, the authors decided to use the mesh with 25-million grid points as it had sufficient accuracy with the maximum efficiency in computational time. The time for one steady-state simulation took less than 5 h on a workstation with 23 cores. Thus, it could be conducted overnight.

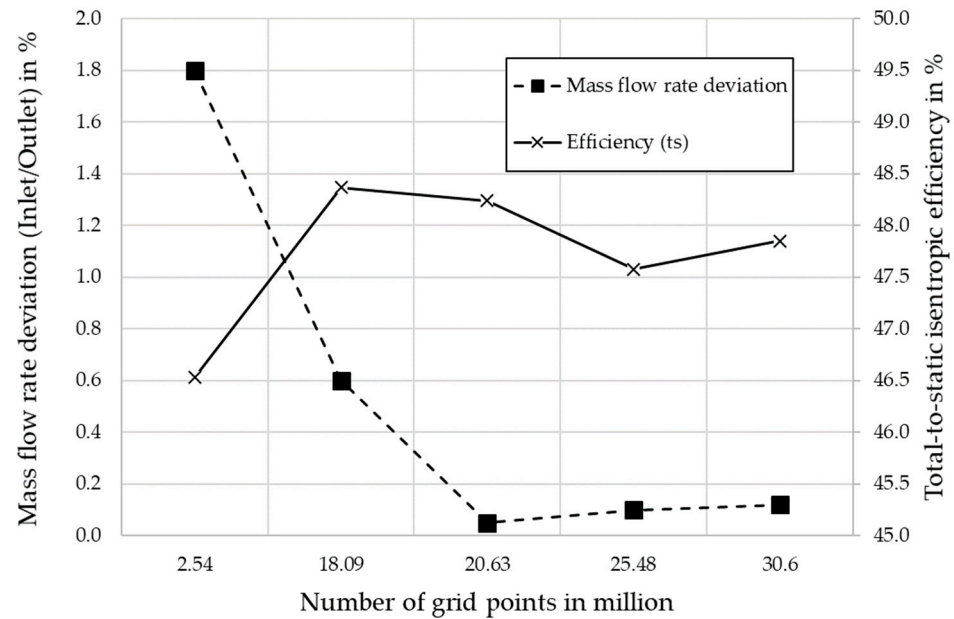


Figure 6. Mass flow rate deviation and total-to-static isentropic efficiency as a function of the number of grid points.

2.3. Initial Turbine Design Data

With the design boundary conditions in Table 3, the following geometric turbine design data (Table 5) were calculated by means of the 1D TDT. Iteratively, after a few iterations, the estimated 1D efficiency (40%, Table 3) almost hit the efficiency calculated by the 1D TDT (39%, Table 5). This is a must for the consistency of the approach.

Table 5. 1D TDT geometric output data for the four-fold MM Elektra turbine.

Parameter	Unit	1D TDT Output	Adapted
Number of blades	-	38	84
Blade relative inlet angle	°	30	30
Blade relative outlet angle	°	150	150
Blade-channel width	mm	3.5	3.5
Blade-height outer diameter	mm	19.7	17.17
Blade-height inner diameter	mm	27.6	19.8
Nozzle throat area	mm ²	111.24	111.24
Nozzle outlet area	mm ²	406.78	406.78
Nozzle length (throat to outlet)	mm	142.42	49.72
Nozzle-inclination angle	°	26.43	26.43
1st wheel-pass degree of admission	%	6.7	6.7
1st deflection-channel inlet angle	°	145.43	145.43
2nd wheel-pass degree of admission	%	9.7	9.7
2nd deflection-channel inlet angle	°	141.35	141.35
3rd wheel-pass degree of admission	%	17.8	17.8
3rd deflection-channel inlet angle	°	135.51	135.51
4th wheel-pass degree of admission	%	50	32
Calculated efficiency, $\eta_{is,ts}$ (1D TDT)	%	39	
Expected shaft power	kW	≈6–7	

Based on the few geometry data, the 3D CAD model of the Elektra turbine was engineered for the following 3D-CFD investigations. Before the first simulations were started, the first adjustments were made directly to the 1D TDT output data (see Table 5 (Adapted)). This was necessary because our experience from former designs of turbines with multiple velocity stages (e.g., pressurized air Elektra [49]) had already shown that the 1D model loss model overpredicts the bucket losses and, therefore overadjusts the increase

of the blade height. Therefore, the blade heights were adjusted according to experience and can also be further adjusted according to the received CFD results. Furthermore, the number of blades was greatly increased, which directly resulted from the specification of the width of the blade channel and the diameter of the rotor. The last adjustment was the degree of admission of the last wheel pass. Here, the degree of admission was reduced from 50% to 32% since the deflection channels would otherwise not have been implementable in CAD for reasons of space.

2.4. CFD Turbine Optimization

The process began with the conversion of 1D TDT-generated geometry data into a 3D CAD model of the turbine. Subsequently, a series of steady 3D Computational Fluid Dynamic (CFD) simulations were conducted, focusing on design boundary conditions. The intention was to maintain consistency throughout the design optimization by applying identical physical models and boundary conditions at each stage, enabling comparisons with previous simulations. The workflow for the numerical investigation was initiated with preprocessing in the Interactive Geometry Generator (IGG) and Autogrid, which were used to generate block-structured grids. IGG was used to generate the blocks for the CD nozzle and the deflection channels and Autogrid for the meshing of the blade channels of the rotor wheel. This splitting of the meshing process was conducted because Autogrid is a tool that is capable of generating a structured mesh-out of the geometry of turbine rotor wheels. The rest of the meshing had to be completed by hand in IGG. After achieving a converged solution using the flow solver, the results were subjected to an analysis in CFView, a program designed for computational flow visualization. The post-processing phase emphasized the evaluation of total and static quantities, with mass flow weighting pertaining to pressure and temperature to derive the total-to-static isentropic efficiency. Additionally, contour plots of the Mach number distribution were employed for a visual assessment of the results. Following an evaluation of the optimization potential, adjustments were made to the turbine's geometry either in the CAD software or directly within IGG, with iterative improvements.

3. Results

In the following, the working fluid-flow phenomena, or geometry optimization, respectively, by CFD is discussed, and the results of the 3D CFD analysis calculations are compared and discussed with original 1D design objectives and 1D calculations. Using the approach mentioned in Section 2.4, four different versions (V1–V4) of the turbine were considered. Figure 7 shows the isentropic efficiency (η_s) of all the versions compared to each other. Table 6 lists the investigated geometry adjustments. The optimization steps are described in more detail below. The authors were successful in improving the turbine's efficiency step by step.

Table 6. Geometry adjustments for the different Elektra versions.

Versions of the Turbine	Changes to the Geometry
V1	–
V2	Smaller nozzle outlet area (406.27 mm ² to 339.6 mm ²), decreased deflection channel (DC) width (20.20 mm to 15.03 mm), improved 3rd deflection channel (outlet from 16% to 8.8% admission), smaller outlet area (12.2% to 9.34% of the circumference)
V3	Flow optimized radius at 2nd DC (radius from 38.23 mm to 35.16 mm), decreased outlet area (9.34% to 6.36% at the outer circumference)
V4	Flow optimization of 2nd deflection channel (decreased channel width from 29.93 mm to 24.81 mm), increased inner DC height (from 18.87 mm to 20 mm)

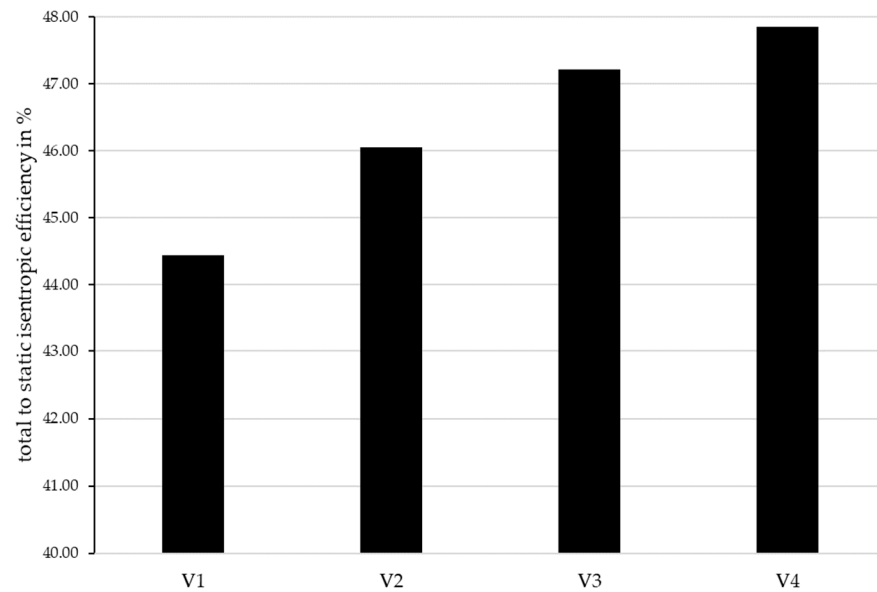


Figure 7. Comparison of the isentropic efficiency (η_s) for four different versions of the Elektra turbine in CFD.

Figure 8 compares the absolute Mach number distribution at a blade height of 50% for the four Elektra versions. The first version, V1 (a) at the top left of the figure, is still in the state with the already adjusted values from the 1D design as described in Table 5. In the overview, the shortage of space, addressed in Section 2.3, regarding the deflection channels become directly clear. For the deflection channels, which are in the inner part of the rotor wheel, it is also directly ensured that a bore for the shaft can be placed in the middle. For this reason, some free space is left in the inner area. Furthermore, it is obvious that the circumferential space outside of the rotor is completely utilized in Version V1. The one CD nozzle inlet is placed only a few millimeters next to the other outlet area of the turbine (see also Figure 1). For this reason, the lower degree of admission of the fourth wheel passage, already described in Section 2.3, was chosen.

A close look at the Mach number distribution of Version V1 (Figure 8a) reveals that the nozzle accelerates continuously, and no flow separation can be seen. However, shortly before entering the blade channel of the rotor, a compression shock occurs, with the velocity dropping abruptly from approximately Mach 2.2 to below Mach 2. The fluid flows through the first wheel passage and enters the first deflection channel relatively homogeneously. After the first deflection in the first deflection channel, there is a strong detachment area and the fluid streams through the blade rows only in approximately half of the admitted area of the second wheel pass. Consequently, the fluid also enters the second deflection channel only in some areas. After the deflection in the second deflection channel, a similar flow separation occurs as in the first deflection channel. Interestingly, the flow through the third wheel pass is relatively homogeneous again—approximately 3/4 of the admitted area is flowed through by the medium. In the third deflection channel, the flow separates from both walls, attaches again at the end of the wall in the direction of rotation, and flows through approximately one third of the admitted area of the fourth wheel pass. Consequently, only a quarter of the outlet area is passed through by the medium. The turbine efficiency for Version V1 was at 44.45%.

Based on this information, the first changes/optimizations to the turbine were implemented, as can be seen in Version V2, Figure 8b. Since the authors assumed that the shockwave at the end of the nozzle was due to overexpansion, the width of the nozzle at the exit, i.e., the nozzle exit area, was reduced. To counteract the flow separation in the first deflection channel, the width of the deflection channel was reduced, just by the width of the separation area. Furthermore, the strong widening of the third deflection channel

towards the fourth wheel pass was reduced (the outlet area then also had to be reduced in circumference). These changes increased the turbine efficiency of Version V2 to 46.05%.

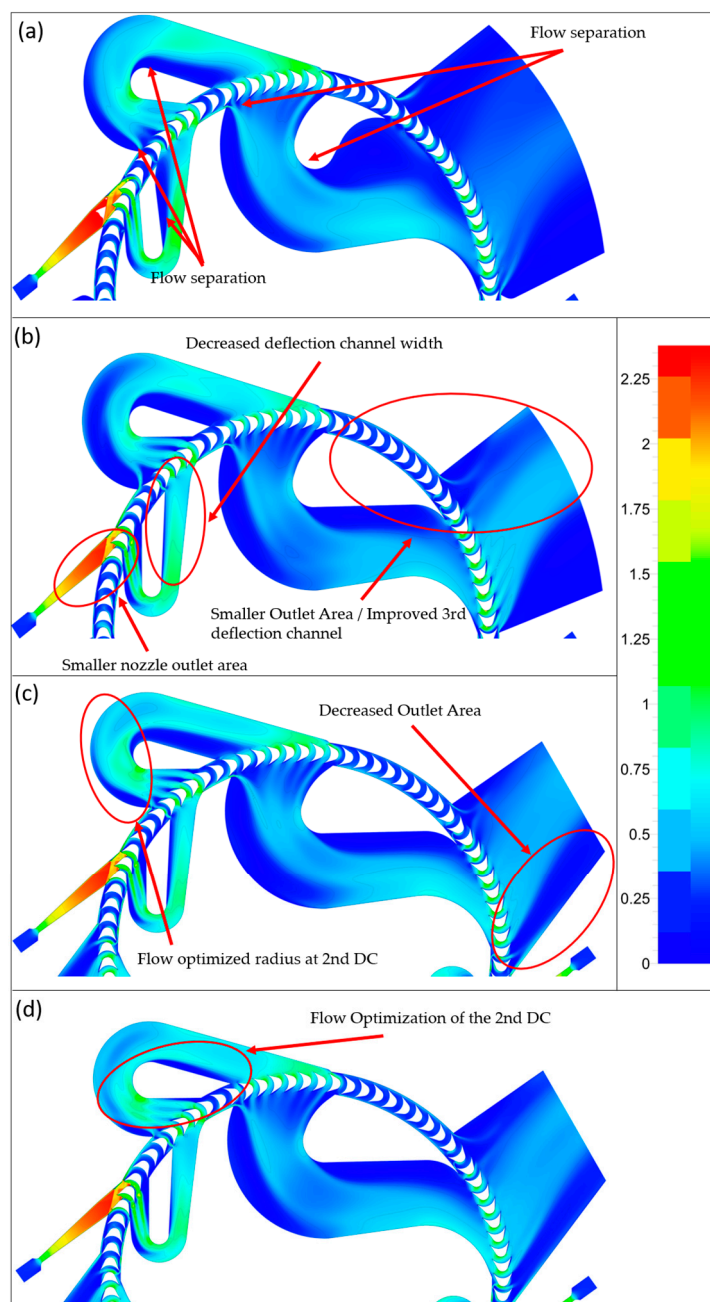


Figure 8. Comparison of CFD simulations results at 50% span: (a) Absolute Mach Number plot of version V1; (b) Absolute Mach Number plot of version V2; (c) Absolute Mach Number plot of version V3; (d) Absolute Mach Number plot of version V4.

However, in this updated Version V2, the problem of strong flow separation in the second deflection channel is still present. Furthermore, the fluid does not use the entire available outlet area. For this reason, Version V3 (Figure 8c) implements a modified outer deflection radius in the second deflection channel and a smaller outlet area. Figure 8c clearly shows that these adjustments produce a more homogeneous flow pattern in the second deflection channel and that the outlet area now also has better flow guidance than in Version V2 before. Through these changes, the turbine efficiency could be again increased to 47.21%. Comparing Version V4 to Version V3, the second deflection channel is now

adapted again to reduce the detachment area after the deflection. This small change also only had a small impact on the turbine efficiency but still increased it by a small amount to 47.85%. It must be pointed out once more that the discussed flow fields are the results of steady-state frozen-rotor simulations. Thus, all unsteady effects like filling or emptying of the flow passages, acceleration, and deceleration of the flow at the beginning and the end of the admitted arc are not considered. Furthermore, tip-leakage flows around the shroud and disc friction of the bucket wheel are also neglected. Based on our recent numerical and experimental investigation of a compressed air Elektra turbine [49], we expect an efficiency deterioration of about 5 p.p.

Parallel to the observation of the Mach number distribution of the flow through the turbine, the static pressure distributions in streamwise direction were evaluated. The values were obtained by mass weighted averaging of surfaces on the certain positions. Figure 9 shows a comparison of the streamwise static pressure distribution of the four CFD versions and the 1D design. It is immediately clear that the streamwise static pressure distribution in the 3D-CFD simulations is consistently higher than the 1D design distribution, up to the outlet. The CD nozzle in the 1D design calculation expands to slightly above exhaust pressure: the 0.5 bar. Downstream, almost equal pressure is achieved for all velocity stages, i.e., wheel passes, respectively. There is a slight pressure increase over the first two wheel passes, probably due to supersonic flow conditions and a slight pressure decrease in the last two passes according to subsonic flow conditions. In comparison, for all 3D-CFD simulations, the static pressure at the nozzle outlet, upstream of the first wheel pass, is approximately one bar. Apparently, the CD nozzle works in a different operating point in 3D CFD than designed in 1D. Downstream, the 3D-CFD pressure increases to approximately 1.2 bars over the first wheel pass and rises again to approximately 1.4 bars over the first deflection channel. From this point on (the inlet second wheel pass), the pressure drops steadily in all 3D CFD simulations.

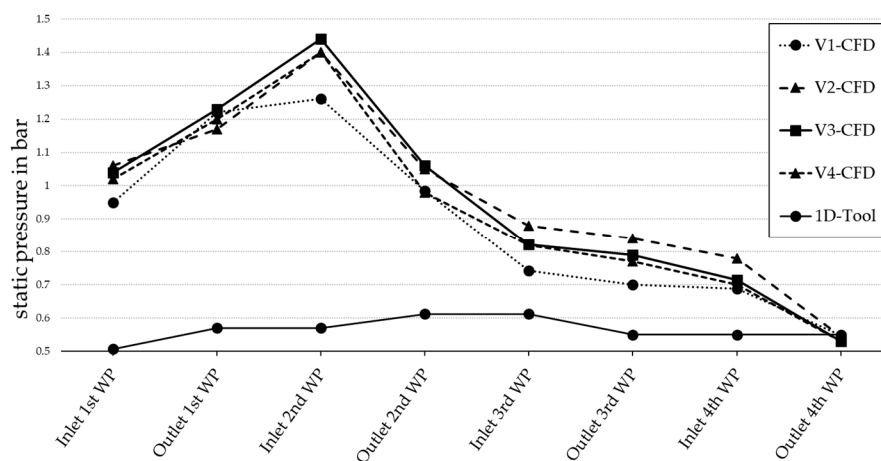


Figure 9. Comparison of the static pressure distribution in streamwise direction through the turbine for the 1D Tool and different CFD calculations.

The strong pressure increases in the first wheel pass and the first deflection channel in the CFD compared to the 1D design appears to be due to the strong flow separation in the deflection channels in the supersonic flow regime, which are not considered by the simple 1D loss model. These large pressure drops build up greater pressure, starting from the turbine outlet upstream to the nozzle exit. Interestingly, the static pressure is at its maximum exactly at the entrance of the second wheel passage. This can be explained by the choked flow at the second wheel passage (Figure 10). Due to the choked flow, the pressure cannot increase further upstream. Upstream of the choked-flow regime, the pressure sets itself according to the mass flow rate and the critical area. The distribution also shows that the four different versions of the CFD simulations do not show significant differences to each other. Thus, the adjustments performed in this work of the flow channels

do not show too much influence on the static pressure profile of the flow. The test turbine currently under construction will be equipped with the necessary pressure tappings. So, this questionable pressure distribution will be measured in the CHP ORC plant in Prague.

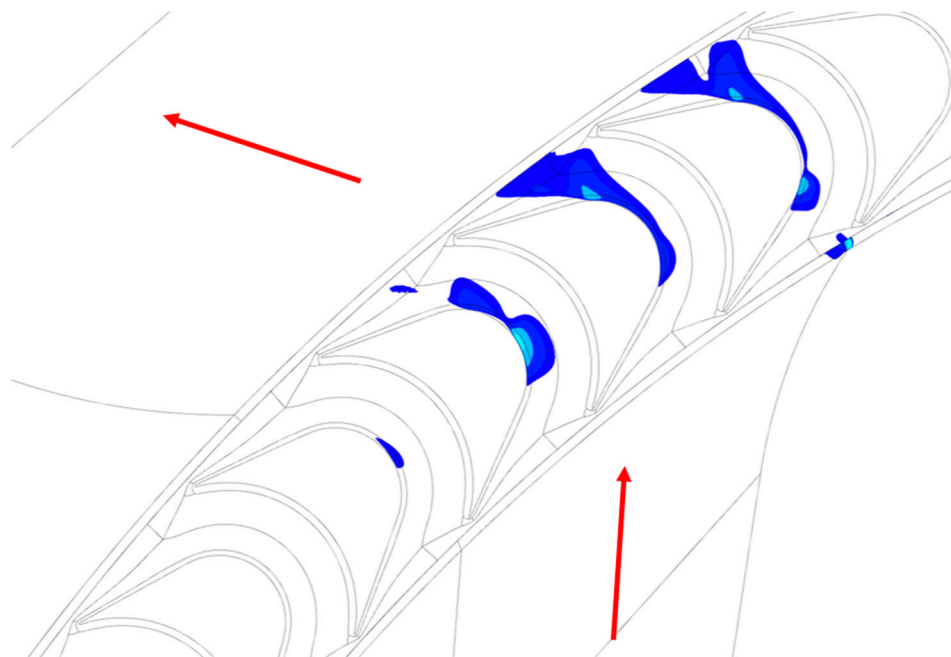


Figure 10. Choked-flow region ($M_{rel} > 1$, in blue) in the bucket passages of the second wheel pass (red arrows show flow direction).

In the next step, the authors decided to investigate the best-performing version, V4, further by conducting off-design CFD calculations of this turbine. Figure 11 shows that the total-to-static isentropic efficiency of Version V4 over the rotational design speed of the turbine is 3000 rpm. The turbine efficiency drops very sharply towards lower speeds, which was to be expected. Of course, due to the four-fold admission of the turbine, the relative inflow angle of the impeller differs from metal blade angle resulting in large incidence losses for each wheel pass for reduced rotational speed. The effect of the incorrect inflow to the rotor is, therefore, much stronger with the four-fold RE-Elektra turbine compared to a simple impulse stage. Towards higher speeds, the efficiency still increases slightly and achieves its maximum at 3500 rpm, which is higher than the design speed. This behavior is not surprising. Equipped with just one velocity stage (i.e., one wheel pass), the turbine would perform best at about 12,000 rpm. Increasing speed for the four velocity stages turbine means that the first pass works more effectively, the others less. The last wheel pass might immediately start to brake. So, we have two counteracting effects, which lead to maximum efficiency—here above the design speed. Since the flow in the Elektra turbine is, of course, highly unsteady (four times partially admitted), a further transient simulation was carried out at the design rotational speed. As can be seen, the efficiency of the unsteady simulation is about 3.5%-points below the steady-state calculation. The transient effects do not seem to have too much influence on the efficiency of the turbine, or the steady-state simulation already has accidentally an adverse position between stator and rotor via its frozen rotor approach. Interestingly, the 1D design efficiency is still below the efficiency of the transient CFD Calculation. This also reconfirms the assumption that the 1D TDT loss model is too pessimistic. Although Figure 11 indicates that Elektra's design goal of approximately 50% efficiency has been achieved yet, it must be emphasized that these efficiencies data rely on a simplified CFD design approach calculations. Efficiencies will be measured in the CHP ORC plant in Prague. The authors expect approximately 5 p.p. less based on their experience [49].

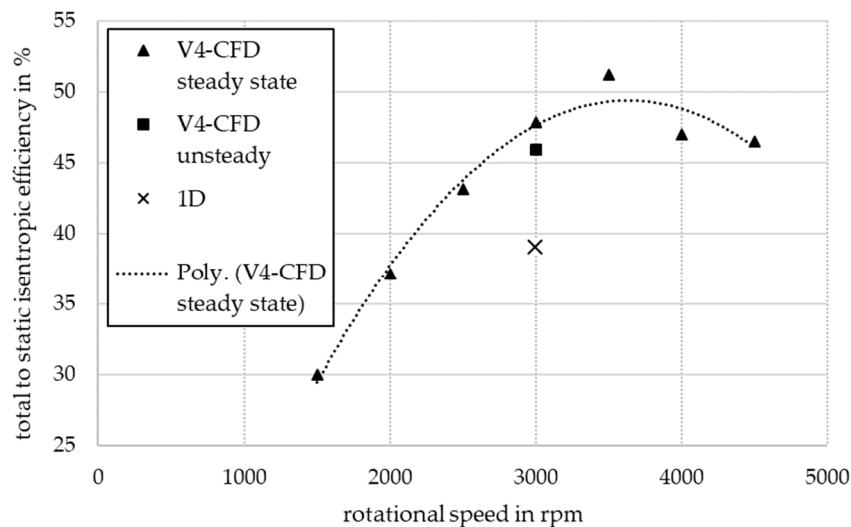


Figure 11. Total-to-static isentropic efficiency as a function of the rotational speed for the V4–CFD steady state, V4–CFD unsteady, and the 1D calculation.

4. Discussion

The results of the CFD simulation show that the 1D TDT gives, at most, a rough suggestion for the design of velocity compounded with the multi RE turbine. Particularly regarding the degree of admission for the last deflection channel/outlet, there must be a major deviation from the specifications of the 1D TDT. This is largely understandable since the tool does not consider the size ratios of the turbine. Due to the relatively small area inside the impeller and the relatively wide deflection channels, the final design is strongly influenced by the space conditions. Furthermore, it becomes clear that the efficiency calculation in the tool deviates strongly from the results in the CFD. This was already mentioned in former publications [49]. Due to the multiple application of the loss model, four times through the wheel passages and three times through the deflection channels, the deviations of the model have an even greater effect here than in previous designs of Elektra turbines with only two wheel passages. Furthermore, the pessimistic loss assessment does not only reduce the predicted efficiency but also over-adjusts the increase in blade height due to overpredicted losses. However, the knowledge already gained by the authors allowed these errors to be corrected directly before the first CFD simulation. The optimization of the turbine directly in the CFD becomes, therefore, indispensable due to the many uncertainties in the 1D model. The relatively simple meshing in combination with the adjustments in CAD again turned out to be a very helpful, practicable approach. The fast design simulations allowed different versions of the turbine to be considered and analyzed in a very short time (approximately one version per day). The changes in the flow variables because of the adjustments to the turbine (flow channel/nozzle) could always be reconstructed in retrospect in the CFD analysis. The adjustments to the nozzle geometry and to the deflection channels—Version V1 to Version V4—were able to steadily improve the efficiency of the turbine from 44.45% to 47.85%. However, it should be noted that none of the adjustments would have had a strong influence on the streamwise pressure distribution in the turbine. The equal-pressure design through the turbine, downstream of the CD nozzles, could thus not be implemented to any extent. Furthermore, the CFD calculations also reach their limits when the flow is strongly unsteady, the flow detaches in parts of the turbine and generally an unclean flow prevails. Nevertheless, this approach was again found to be acceptable to identify tendencies in optimization and efficiency increase between the different versions.

5. Conclusions

As the experimental verification of the velocity compounded RFFRE-T is still pending, the research questions posed in the introduction can only be answered provisionally. Based on the 3D CFD investigations for the 7 kW_{el} MM turbine under consideration, it became apparent that achieving 50% expansion efficiency with the Elektra turbine concept is questionable (question 1). Although efficiencies in the range of 45–50% were calculated, these were only achieved by neglecting the gap losses and unsteady flow effects. For machines with 30–50 kW_{el}, achieving the 50% target does not seem impossible (Question 3). To achieve this, however, the design chain must be significantly improved. Currently, the 1D TDT only gives very rough indications. It may be necessary to abandon this approach altogether and to aim for an adjoint flow solver i.e., a numerical optimization tool.

The second research question, addressing manufacturing and operational costs, can only be answered by manufacturing, and testing the MM Elektra turbine. Thus, the authors have decided that the next step is to completely engineer the Elektra version V4 in CAD and have it manufactured. The manufactured turbine will then be installed and tested under real field conditions in the woodchips-fired CHP ORC plant [53,54] at CTU UCEEB and compare the CFD predictions with reality, regarding both efficiency and pressure distribution over a certain operation range. Since this plant is currently operating with a 3000 rpm rotary vane expander, direct comparisons with the Elektra turbine regarding wear, vibrations, etc. can be made there as well.

Author Contributions: Conceptualization, A.P.W. and V.N.; Data curation, P.S.; Funding acquisition, J.Š. and V.N.; Investigation, P.S. and D.S. Methodology, P.S., A.P.W. and D.S. Project administration, J.Š. and V.N.; Software, P.S. and D.S. Supervision, A.P.W., V.N. and M.K.; Visualization, P.S.; Writing—original draft, P.S. and A.P.W.; Writing—review & editing, P.S., A.P.W., D.S., J.Š., L.B.A., V.N. and M.K. All authors have read and agreed to the published version of the manuscript.

Funding: The research leading to these results has received funding from the EEA Grants and the Technology Agency of the Czech Republic within the KAPPA Programme. Project code TO01000160.

Data Availability Statement: The data presented in this study are available on request from the corresponding author. The data are not publicly available due to amount and size of data.

Conflicts of Interest: The authors declare no conflicts of interest. The funders had no role in the design of the study; in the collection, analyses, or interpretation of data; in the writing of the manuscript, or in the decision to publish the results.

Nomenclature

A	area (mm ²)
β	relative flow angle (°)
c	absolute velocity (m·s ⁻¹)
Δ	difference (1)
D	diameter (mm)
ε	degree of admission (%)
h	specific enthalpy (J·kg ⁻¹)
h	blade height (mm)
η	efficiency (%)
n	rotational speed (rpm)
p	pressure (Pa)
T	temperature (K)
P	power (kW)
u	circumferential velocity (m·s ⁻¹)
w	relative velocity (m·s ⁻¹)

Subscripts	
el	electrical
is	isentropic
in	inner
opt	optimum
out	outer, outlet
ts	total-to-static
0	total
rel	relative
Abbreviations	
CAD	computer aided design
CD	convergent-divergent
CFD	computational fluid dynamics
CHP	combined heat and power
CSP	concentrated solar power
DC	deflection channel
IGG	internal grid generator
MM	hexamethyldisiloxane
MS	Microsoft
MTG-c	micro turbine generator construction
ORC	Organic Rankine cycle
P2H2P	power to heat to power
PR	pressure ratio
RANS	Reynolds averaged Navier Stokes
ROT	Radial outflow turbine
RE	Re-entry
RFFRE-T	Radial four fold re-entry turbine
SA	Spalart-Allmaras
VRAT	volume flow ratio
WHR	waste heat recovery
WP	wheel pass
1D	one dimensional
1D TDT	one dimensional turbine design tool
3D	three dimensional

References

1. Meher-Homji, C.B. The Historical Evolution of Turbomachinery. In Proceedings of the 29th Turbomachinery Symposium 2000, Houston, TX, USA, 29 September 2000; pp. 281–322. [\[CrossRef\]](#)
2. Tartière, T.; Astolfi, M. A World Overview of the Organic Rankine Cycle Market. *Energy Procedia* **2017**, *129*, 2–9. [\[CrossRef\]](#)
3. Tocci, L.; Pal, T.; Pasmazoglou, I.; Franchetti, B. Small Scale Organic Rankine Cycle (ORC): A Techno-Economic Review. *Energies* **2017**, *10*, 413. [\[CrossRef\]](#)
4. Lemort, V.; Ludovic, G.; Arnaud, L.; Declaye, S.; Quoilun, S. A comparison of piston, screw and scroll expander for small Rankine cycle systems. In Proceedings of the 3rd International Conference on Microgeneration and Related Technologies, Naples, Italy, 15–17 April 2013.
5. Glavatskaya, Y.; Podevin, P.; Lemort, V.; Shonda, O.; Descombes, G. Reciprocating Expander for an Exhaust Heat Recovery Rankine Cycle for a Passenger Car Application. *Energies* **2012**, *5*, 1751–1765. [\[CrossRef\]](#)
6. Weiß, A.P. Volumetric expander versus turbine—Which is the better choice for small ORC plants? In *ASME-ORC2015, Proceedings of the 3rd International Seminar on ORC Power Systems, Brussels, Belgium, 12–14 October 2015*; University of Liège: Liège, Belgium; Ghent University: Ghent, Belgium, 2015; ISBN 978-2-9600059-2-9.
7. Weiß, A.P.; Popp, T.; Müller, J.; Hauer, J.; Brüggemann, D.; Preißinger, M. Experimental characterization and comparison of an axial and a cantilever micro-turbine for small-scale Organic Rankine Cycle. *Appl. Therm. Eng.* **2018**, *140*, 235–244. [\[CrossRef\]](#)
8. Uusitalo, A.; Zocca, M.; Turunen-Saaresti, T. *Measurement System of Small-Scale High Expansion Ratio ORC Turbine*; Springer: Berlin/Heidelberg, Germany, 2021; pp. 114–122.
9. Kaczmarczyk, T.Z.; Żywica, G.; Ilnatowicz, E. Experimental Investigation of a Radial Microturbine in Organic Rankine Cycle System with HFE7100 as Working Fluid. In Proceedings of the 3rd International Seminar on ORC Power Systems, Brussels, Belgium, 12–14 October 2015; pp. 1–10.
10. Popp, T.; Weiß, A.P.; Heberle, F.; Winkler, J.; Scharf, R.; Weith, T.; Brüggemann, D. Experimental Characterization of an Adaptive Supersonic Micro Turbine for Waste Heat Recovery Applications. *Energies* **2021**, *15*, 25. [\[CrossRef\]](#)

11. Sun, H.; Li, H.; Gao, P.; Hou, F.; Hung, T.-C.; Chang, Y.-H.; Lin, C.-W.; Qin, J. Numerical simulation and low speed experiment of a low partially admitted rate axial turbine for small scale organic Rankine cycle. *Appl. Therm. Eng.* **2024**, *238*, 122002. [[CrossRef](#)]
12. Bahamonde, S.; Pini, M.; de Servi, C.; Rubino, A.; Colonna, P. Method for the Preliminary Fluid Dynamic Design of High-Temperature Mini-Organic Rankine Cycle Turbines. *J. Eng. Gas Turbines Power* **2017**, *139*, 082606. [[CrossRef](#)]
13. Casati, E.; Vitale, S.; Pini, M.; Persico, G.; Colonna, P. Centrifugal Turbines for Mini-Organic Rankine Cycle Power Systems. *J. Eng. Gas Turbines Power* **2014**, *136*, 122607. [[CrossRef](#)]
14. Żywica, G.; Kaczmarczyk, T.; Ichnatowicz, E.; Bagiński, P.; Andrearczyk, A. Design and manufacturing of micro-turbomachinery components with application of heat resistant plastics. *Mech. Mech. Eng.* **2018**, *22*, 649–660. [[CrossRef](#)]
15. Żywica, G.; Kaczmarczyk, T.Z.; Breńkacz, Ł.; Bogulicz, M.; Andrearczyk, A.; Bagiński, P. Investigation of dynamic properties of the microturbine with a maximum rotational speed of 120 krpm—Predictions and experimental tests. *J. Vibroeng.* **2020**, *22*, 298–312. [[CrossRef](#)]
16. Riffat, S.B.; Zhao, X. A novel hybrid heat-pipe solar collector/CHP system—Part II: Theoretical and experimental investigations. *Renew. Energy* **2004**, *29*, 1965–1990. [[CrossRef](#)]
17. Hernandez-Carrillo, I.; Wood, C.; Liu, H. Development of a 1000 W organic Rankine cycle micro-turbine-generator using polymeric structural materials and its performance test with compressed air. *Energy Convers. Manag.* **2019**, *190*, 105–120. [[CrossRef](#)]
18. Pu, W.; Yue, C.; Han, D.; He, W.; Liu, X.; Zhang, Q.; Chen, Y. Experimental study on Organic Rankine cycle for low grade thermal energy recovery. *Appl. Therm. Eng.* **2016**, *94*, 221–227. [[CrossRef](#)]
19. Li, M.; Wang, J.; He, W.; Gao, L.; Wang, B.; Ma, S.; Dai, Y. Construction and preliminary test of a low-temperature regenerative Organic Rankine Cycle (ORC) using R123. *Renew. Energy* **2013**, *57*, 216–222. [[CrossRef](#)]
20. Pei, G.; Li, J.; Li, Y.; Wang, D.; Ji, J. Construction and dynamic test of a small-scale organic rankine cycle. *Energy* **2011**, *36*, 3215–3223. [[CrossRef](#)]
21. Nguyen, V.M.; Doherty, P.S.; Riffat, S.B. Development of a prototype low-temperature Rankine cycle electricity generation system. *Appl. Therm. Eng.* **2001**, *21*, 169–181. [[CrossRef](#)]
22. Yagoub, W.; Doherty, P.; Riffat, S.B. Solar energy-gas driven micro-CHP system for an office building. *Appl. Therm. Eng.* **2006**, *26*, 1604–1610. [[CrossRef](#)]
23. Klonowicz, P.; Heberle, F.; Preißinger, M.; Brüggemann, D. Significance of loss correlations in performance prediction of small scale, highly loaded turbine stages working in Organic Rankine Cycles. *Energy* **2014**, *72*, 322–330. [[CrossRef](#)]
24. Shao, L.; Zhu, J.; Meng, X.; Wei, X.; Ma, X. Experimental study of an organic Rankine cycle system with radial inflow turbine and R123. *Appl. Therm. Eng.* **2017**, *124*, 940–947. [[CrossRef](#)]
25. Seume, J.R.; Peters, M.; Kunte, H. Design and test of a 10 kW ORC supersonic turbine generator. *J. Phys. Conf. Ser.* **2017**, *821*, 12023. [[CrossRef](#)]
26. Kosowski, K.; Piwowarski, M.; Stepień, R.; Włodarski, W. Design and investigations of the ethanol microturbine. *Arch. Thermodyn.* **2018**, *39*, 41–54. [[CrossRef](#)]
27. Rosset, K.; Pajot, O.; Schiffmann, J. Experimental investigation of a small-scale organic rankine cycle turbo-generator supported on gas-lubricated bearings. *J. Eng. Gas Turbines Power* **2021**, *143*, 051015. [[CrossRef](#)]
28. Gazet, C.; Leroux, A.; Paillette, B.; Pauchet, A. Operational experience on ORC use for waste heat valorization in biogas power plant. In Proceedings of the 3rd International Seminar on ORC Power Systems, Brussels, Belgium, 12–14 October 2015; pp. 1–7.
29. Yue, C.; Huang, Y.; Wu, Y. Experimental Study of Low-temperature Organic Rankine Cycle with Axial Flow Turbine. *Energy Procedia* **2015**, *75*, 1583–1589. [[CrossRef](#)]
30. Guillaume, L.; Legros, A.; Desideri, A.; Lemort, V. Performance of a radial-inflow turbine integrated in an ORC system and designed for a WHR on truck application: An experimental comparison between R245fa and R1233zd. *Appl. Energy* **2017**, *186*, 408–422. [[CrossRef](#)]
31. Demierre, J.; Favrat, D.; Schiffmann, J.; Wegele, J. Experimental investigation of a Thermally Driven Heat Pump based on a double Organic Rankine Cycle and an oil-free Compressor-Turbine Unit. *Int. J. Refrig.* **2014**, *44*, 91–100. [[CrossRef](#)]
32. Cho, S.-Y.; Cho, C.-H.; Choi, S.-K. Experiment and cycle analysis on a partially admitted axial-type turbine used in the organic Rankine cycle. *Energy* **2015**, *90*, 643–651. [[CrossRef](#)]
33. Jubori, A.M.A.; Al-mousawi, F.N.; Rahbar, K.; Al-dadah, R. Design and manufacturing a small-scale radial-inflow turbine for clean organic Rankine power system. *J. Clean. Prod.* **2020**, *257*, 120488. [[CrossRef](#)]
34. Weiß, A.P.; Popp, T.; Zinn, G.; Preißinger, M.; Brüggemann, D. A micro-turbine-generator-construction-kit (MTG-c-kit) for small-scale waste heat recovery ORC-Plants. *Energy* **2019**, *181*, 51–55. [[CrossRef](#)]
35. Somerscales, E.F.C. The Vertical Curtis Steam Turbine. *Trans. Newcom. Soc.* **1990**, *62*, 157–158. [[CrossRef](#)]
36. Rezaie, B.; Rosen, M.A. District heating and cooling: Review of technology and potential enhancements. *Appl. Energy* **2012**, *93*, 2–10. [[CrossRef](#)]
37. Cruz, I.; Johansson, M.T.; Wren, J. Assessment of the potential for small-scale CHP production using Organic Rankine Cycle (ORC) systems in different geographical contexts: GHG emissions impact and economic feasibility. *Energy Rep.* **2022**, *8*, 7680–7690. [[CrossRef](#)]
38. Branchini, L.; dePascale, A.; Melino, F.; Torricelli, N. Optimum Organic Rankine Cycle Design for the Application in a CHP Unit Feeding a District Heating Network. *Energies* **2020**, *13*, 1314. [[CrossRef](#)]

39. Prando, D.; Renzi, M.; Gasparella, A.; Baratieri, M. Monitoring of the energy performance of a district heating CHP plant based on biomass boiler and ORC generator. *Appl. Therm. Eng.* **2015**, *79*, 98–107. [[CrossRef](#)]
40. Klonowicz, P.; Fijałkowski, T.; Antczak, Ł.; Magiera, R. Radial Curtis Stage. In Proceedings of the 10th Conference on Power System Engineering, Thermodynamics & Fluid Flow, Pilsen, Czech Republic, 16–17 June 2011.
41. Kolb, O. Elastic Fluid Turbine. U.S. Patent US842211A, 29 January 1907.
42. Ladewig, H. Ladewig spricht über die Elektra-Dampfturbine. *Z. Des Ver. Dtsch. Ingenieure* **1906**, *35*, 1415–1416.
43. Meuth, H. The Elektra Steam Turbine. *J. Am. Soc. Nav. Eng.* **1910**, *22*, 402–416. [[CrossRef](#)]
44. Stodola, A. *Die Dampfturbinen*, 3rd ed.; Springer: Berlin/Heidelberg, Germany, 1905; ISBN 978-3-66-236141-2.
45. Evans, D.G. *Nasa Memorandum: Design and Experimental Investigation of a Three-Stage Multiple-Reentry Turbine*; NASA: Cleveland, OH, USA, 1959.
46. Linhardt, H.D. *Study of Turbine and Turbopump Design Parameters: A Study of High Pressure Ratio Re-Entry Turbines*; NASA: Pacoima, CA, USA, 1960.
47. Linhardt, H.D. Re-Entry Turbines for Secondary Space Power Systems. *ARS J.* **1962**, *32*, 1552–1560. [[CrossRef](#)]
48. Kryłłowicz, W.; Liśkiewicz, G.; Szwaja, S. Konstrukcja malej turbiny parowej typu Elektra dla energetyki rozproszonej. *Energetyka* **2015**, *11*, 719–722.
49. Weiß, A.P.; Stümpfl, D.; Streit, P.; Shoemaker, P.; Hildebrandt, T. Numerical and Experimental Investigation of a Velocity Compounded Radial Re-Entry Turbine for Small-Scale Waste Heat Recovery. *Energies* **2022**, *15*, 245. [[CrossRef](#)]
50. Weiß, A.P.; Novotný, V.; Popp, T.; Streit, P.; Špale, J.; Zinn, G.; Kolovratník, M. Customized ORC micro turbo-expanders—From 1D design to modular construction kit and prospects of additive manufacturing. *Energy* **2020**, *209*, 118407. [[CrossRef](#)]
51. Moustapha, H.; Zelesky, M.F. *Axial and Radial Turbines*; Concepts NREC: White River Junction, VT, USA, 2003; ISBN 0933283121.
52. Lemmon, E.W.; Huber, M.L.; McLinden, M.O. (Eds.) *NIST Standard Reference Database 23: Reference Fluid Thermodynamic and Transport Properties-REFPROP, Version 9.1*; National Institute of Standards and Technology: Gaithersburg, MD, USA, 2013.
53. Mascuch, J.; Novotny, V.; Vodicka, V.; Zeleny, Z.; Spale, J. Set-up and pilot operation of an in-house developed biomass ORC μ CHP in the Czech Republic. In Proceedings of the 5th International Seminar on ORC Power Systems, Athens, Greece, 9–11 September 2019.
54. Mascuch, J.; Novotny, V.; Spale, J.; Vodicka, V.; Zeleny, Z. Experience from set-up and pilot operation of an in-house developed biomass-fired ORC microcogeneration unit. *Renew. Energy* **2021**, *165*, 251–260. [[CrossRef](#)]
55. Products | CFD Solutions: Turbo. Available online: <https://www.numeca.de/en/products-cfd-solutions/> (accessed on 7 October 2021).
56. Hirsch, C.; Lacor, C.; Rizzi, A.; Eliasson, P.; Lindblad, I.; Haeuser, J. *A Multiblock/Multigrid Code for the Efficient Solution of Complex 3D Navier-Stokes Flows*; ESA, Aerothermodynamics for Space Vehicles: Paris, France, 1991; pp. 415–420.
57. Jameson, A.; Schmidt, W.; Turkel, E. Numerical solution of the Euler equations by finite volume methods using Runge Kutta time stepping schemes. In Proceedings of the 14th Fluid and Plasma Dynamics Conference, Palo Alto, CA, USA, 23–25 June 1981; American Institute of Aeronautics and Astronautics: Reston, VA, USA, 1981.

Disclaimer/Publisher’s Note: The statements, opinions and data contained in all publications are solely those of the individual author(s) and contributor(s) and not of MDPI and/or the editor(s). MDPI and/or the editor(s) disclaim responsibility for any injury to people or property resulting from any ideas, methods, instructions or products referred to in the content.